X-RAYING CHEMICAL EVOLUTION AND GALAXY FORMATION IN THE ANTENNAE

G. Fabbiano , A. Baldi , A. R. King , T. J. Ponman , J. Raymond , A. Read , A. Rots , François Schweizer , A. Zezas

¹Harvard-Smithsonian Center for Astrophysics, 60 Garden Street, Cambridge, MA 02138; gfabbiano@cfa.harvard.edu; azezas@cfa.harvard.edu, arots@cfa.harvard.edu
 ²Theoretical Astrophysics Group, University of Leicester, Leicester LE1 7RH, UK; ark@astro.le.ac.uk
 ³ School of Physics & Astronomy, University of Birmingham, Birmingham B15 2TT, UK; tjp@star.sr.bham.ac.uk

⁴Carnegie Observatories, 813 Santa Barbara St., Pasadena, CA 91101-1292; schweizer@ociw.edu

Draft version December 19, 2018

ABSTRACT

We present the integrated 411 ks Chandra ACIS-S exposure of the Antennae galaxies (NGC 4038/39). Besides a rich population of point-like sources, this spectacular image reveals a spatially and spectrally complex hot diffuse gaseous component. For the first time we detect intense line emission from Fe, Ne, Mg and Si in The Antennae, and obtain a detailed picture of spatially varied metal abundances in the hot interstellar medium (ISM) of a galaxy. In certain regions, the abundances of α -elements may be many times solar, while the Fe abundance is sub-solar or near-solar. The differences in the local metal enrichment of the hot ISM may be related to the local star formation rates and to the degree of confinement of the enriched hot ISM. We also report large-scale gaseous features, including two gigantic, ~ 10 -kpc-scale 'loops' extending to the South of the merging disks, and a low-surface-brightness hot halo, extending out to ~ 18 kpc. These features may be related to superwinds from the starburst in The Antennae or result from the merger hydrodynamics. Their long cooling times suggest that they may persist to form the hot X-ray halo of the emerging elliptical galaxy.

Subject headings: galaxies: peculiar — galaxies: individual(NGC4038/39) — galaxies: interactions — X-rays: galaxies — X-ray: ISM

1. INTRODUCTION

The interacting pair of galaxies NGC 4038/39 (The Antennae), at a distance of 19 Mpc ($H_0 = 75$), has been studied intensely at all wavelengths as the nearest example of galaxies undergoing a major merger (e.g., Whitmore et al. 1999; Hibbard et al. 2001; Neff & Ulvestad 2000; Wilson et al. 2000; Fabbiano et al. 2001). The Antennae provide a local laboratory where astronomers can easily observe phenomena that occur in the deeper Universe. There, merging is common and may be an important step in the evolution of galaxies (e.g., Navarro, Frenk & White 1995).

The Antennae have been studied in X-rays since their first observation with Einstein (Fabbiano & Trinchieri 1983). The first Chandra ACIS-S (Weisskopf et al. 2000) observation of this system in December 1999 revealed both a population of exceptionally luminous point-like sources and complex hot diffuse emission with temperatures in the range $kT \approx 0.3-0.8$ keV. This hot gaseous emission is particularly luminous in the regions with the most active star formation (Fabbiano et al. 2001; Zezas et al. 2002a, b; Zezas & Fabbiano 2002; Fabbiano et al. 2003c). Based on these results, our team was awarded a deep monitoring campaign of The Antennae with *Chandra*, which took place in 2001–2002, and vielded a total 114 hr exposure. including the original 1999 December data. Preliminary reports of spectral and flux variability of the most luminous X-ray sources in The Antennae are given in Fabbiano et al. (2003a, b).

In this Letter we present the entire deep data set and give a first report on the spectral analysis of the diffuse

emission, made possible by the exceptional signal-to-noise ratio of our spectra. The main result is the discovery of large spatial variations and enhancements of the metal abundances. Previous attempts at measuring the metallicity of the hot ISM with the December 1999 data were inconclusive (Fabbiano et al. 2003c). We also report on the large-scale properties of the diffuse emission: While the first *Chandra* observations already suggested gaseous diffuse emission south of the system (Fabbiano et al. 2001), the new deep image reveals complex large-scale features.

2. DEEP chandra IMAGE OF THE ANTENNAE

Together with the original observation, the total Chandra ACIS-S exposure on The Antennae is 411 ks, after background flare screening. The standard Level 2 event files obtained by the Standard Data Processing (SDP) were used. The data set consists of seven observations (ObsID: 315, 3040, 3041, 3042, 3043, 3044, 3718). Figure 1 shows the astrometry-corrected and co-added 'raw' data. Details of the data reduction procedures are given in Fabbiano et al. (2003a), Zezas et al. (2003, in preparation) and Baldi et al. (2003, in preparation). CIAO v3.0.1 and XSPEC were used for the data analysis. The latest ACIS gain calibration was applied. Figure 2 shows an adaptively-smoothed true-color image, obtained from data in the 0.3-0.65, 0.65-1.5 and 1.5-6.0 keV energy bands. This spectacular image shows both a population of pointlike sources and diffuse emission with a variety of spatial scales and spectral colors. We will discuss elsewhere our detailed results on the point-source population (Zezas et al. 2003, in preparation). In summary, we detect 120 Fabbiano et al.

sources (3σ) , with 0.3–10.0 keV luminosities in the range $\sim 2 \times 10^{37}$ – 5×10^{39} erg s⁻¹ for an assumed power-law spectrum with $\Gamma = 1.7$ and $N_{\rm H} = 3.4 \times 10^{20} {\rm cm}^{-2}$ (Galactic). Of the sources more luminous than the Eddington luminosity of a neutron star $(3 \times 10^{38} {\rm erg \ s}^{-1})$, $\sim 70\%$ are variable

Below, we concentrate on the most striking features of the diffuse soft emission, which is detected mostly below 1.5 keV. Because of its spectrum, this emission is likely to be thermal emission from hot plasmas (Fabbiano et al. 2001, 2003c). Figures 1 and 2 show that this emission is most intense in those areas within the optical bodies of the galaxies that coincide with the most actively star-forming regions. Figure 2 illustrates that this hot ISM is rich in features, both spatially and spectrally, as suggested by the varied range of X-ray colors. Larger-scale, more diffuse emission is also present, and includes two 10 kpc-size (110" at D=19 Mpc) loop-like structures extending to the south of the main body of emission.

3. METAL ABUNDANCES OF THE HOT ISM

The X-ray spectra extracted from different regions of the hot ISM show a variety of continuum shapes and line-emission strengths (see Baldi et al. 2003 for a complete study). In particular, besides the Fe-L complex (~0.65–1.15 keV), lines of Ne X (0.92 keV), Mg XI-XII (1.34–1.47 keV), and Si XIII-XIV (1.85–2.01 keV) are visible in some of the spectra. Figure 3 shows a metallicity map of the hot ISM. The abundance of the above elements varies widely in different regions, exceeding in places that of our local solar neighborhood. Chandra observations of the dwarf starburst galaxy NGC 1569 have led to the detection of large-scale metal-enriched hot winds (Martin et al. 2002). Our deep Chandra data allow for the first time the detailed correlation of metal abundances with different galaxian regions and the stellar populations.

Table 1 summarizes the spectral properties of three regions (out of 21 regions studied in Baldi et al. 2003), representative of the range of abundances. They are marked in Figure 3 with '1', '5' and '7'. We follow the numbering convention of Baldi et al. (2003) for these regions, and we name them with R1, R5 and R7 in this paper. We fitted the spectra using the most complete thermal model available to us, the APEC model (Smith et al. 2001). An intrinsic variable N_H was fitted, in addition to the fixed line-of-sight Galactic N_H . A power-law was also included in the fits to represent harder sources such as undetected X-ray binaries or young supernova remnants (SNR), and yielded best-fit Γ in the range 1.8–2. Table 1 also lists mean stellar ages of the regions, estimated via a numberweighted average of the mean ages of highly reddened, extremely young clusters (4 Myr; Zhang, Fall, & Whitmore 2001) and young blue clusters (15 Myr; Whitmore et al. 1999), and the relative strength of the star formation rate (SFR) as measured by the index $(U+H\alpha)/(V+I)$.

R1 consists of two metal-poor regions in the northern loop of the disk of NGC 4038. Figures 1 and 2 show a plume extending out of NGC 4038 near the western region, suggesting possible outflows. R5, within the disk of NGC 4038, is a half-shell feature of the hot ISM and has the most impressive emission lines. The spectrum and best-fit model (with residuals) are shown in Figure 4. This

region is also the one with the highest relative SFR and, given its small area, the largest SFR per unit area. R7 is the absorbed region corresponding to the CO-rich "Overlap Region," where the most recent, intense star formation is occurring (Wilson et al. 2000; see Fabbiano et al. 2003c). The mean age of this region is based on optically detected clusters, so it may represent an upper limit on the stellar age of the inner obscured regions. The relative SFR is large, but not as high as that of R5.

In both R5 and R7 the α -elements are relatively more prominent than Iron, consistent with enrichment by the SNe of type II expected in a young stellar population. While we cannot draw any strong conclusions based on only three points, Table 1 may suggest a trend between relative SFR and α -element abundances. The low abundances of R1 may also in part be due to the presence of outflows, which may disperse the element-enriched hot ISM outside of the galaxy.

While the presence of metals in the hot ISM is certain, the values of the abundances are somewhat modeldependent. For the static model, the radiative cooling time $(2 \times 10^7 \text{ years})$ is longer than the relevant recombination time $(2 \times 10^5 \text{ years})$, and it is self-consistent to assume ionization equilibrium. If the X-rays come from a collection of SNRs, there could be some departure from equilibrium, but overionized and underionized regions will tend to cancel out. If there is a wind, there could be significant adiabatic cooling, so the ionization state would be that appropriate for a higher temperature and abundances could be overestimated (e.g., Breitschwerdt 2003). That might affect the derived abundances for the low-temperature regions far out in the halo, but high density regions such as R5 should not be greatly affected. R5 is remarkable for its high concentration of young star clusters. It is possible that the young clusters are still injecting kinetic energy predominantly by means of stellar winds in this region, and that the temperature will increase as the SN rate increases (Gilbert 2002). It seems equally likely that the heated gas has entrained a large amount of cooler material, and that as the region evolves the mean temperature will increase as the cool material is blown away.

4. LARGE-SCALE DIFFUSE EMISSION

At larger radii, Fig. 2 shows soft diffuse emission without any obvious stellar/optical counterparts (Ponman et al. 2003, in preparation). We can identify two components of this emission: (i) two spectacular extended structures, suggesting giant loops or bubbles of hot plasma (the loops, hereafter), ~ 10 kpc across, extending South of NGC 4039, and (ii) a low-surface-brightness soft halo in the region surrounding the stellar disks of the merging galaxies, extending out to at least 18 kpc ($\sim 200''$) from the nucleus of NGC 4039. The latter is not clearly shown in Figure 2, but is revealed at high significance by comparisons of the radial distribution of the X-ray counts, with those expected from a field background (Fig. 5).

The spectra of the loops can be fitted with a thermal plasma with kT varying between 0.29 keV and 0.34 keV (1σ errors of typically 0.01 to 0.03 keV) and metallicities apparently sub-solar (typically 0.1–0.2 solar). The extent and spectral parameters of the low-surface-brightness halo are uncertain because of the uncertainties of the

background subtraction at these large radii. However, the spectra are soft, with nominal kT = 0.23 + 0.02/ $0.01 (1\sigma)$ keV, so this larger-scale emission may be cooler than that of the loops. The best-fit metallicity is only 0.04 solar, and is < 0.13 at 90% confidence in the outer annulus. However, the signal-to-noise ratio of the data is lower than for the hot ISM, and the fits include data from large regions. While we have no reason to believe that the intrinsic spectral parameters vary significantly at these radii, we cannot exclude it either. Hence, these abundances are uncertain. Taken at face value, there is a trend of decreasing abundances going from the hot ISM of the star-forming regions to the loops, and to the larger-scale emission. This trend may be consistent with a picture in which the hot gas in the large-scale halo may have been diluted with metal-poor ambient ISM. The temperature also seems to decrease at large radii, which may be due to adiabatic expansion.

What causes these large-scale features? The extended halo may be the aftermath of superwinds from The Antennae, perhaps resulting from a starburst at the firstencounter epoch $\sim (2-5) \times 10^8 \text{yr}$ ago (Barnes 1988; Mihos et al. 1993; Whitmore et al. 1999) and the prolonged elevated star-formation rate $(4-6 \text{ M}_{\odot}/\text{yr})$ of the past ~ 150 Myr (Mihos, Bothun, & Richstone 1993, esp. Fig. 10). The cooling times in these diffuse regions are ~ 1 Gyr. The thermal energy content of both halo and loops is $\sim 10^{56}$ erg, comparable to the energy of 10^5 SNe. Given the age of the starburst of $\sim 10^8 \text{yr}$, a SN rate of 0.001 per year could have provided this energy. This is a small fraction of the current SN rate of The Antennae (0.2–0.3 yr⁻¹; Neff & Ulvestad 2000) and, likely, of the average rate during the past \sim 150 Mvr.

A simple order-of-magnitude estimate of the expansion velocity of the loops, assuming a 10 kpc extent and constant velocity over a period of $10^7 - 10^8$ yr, yields a velocity of 1000–100 km/s. At least velocities $\gtrsim 300$ km/s are likely to exceed the escape velocity of the system and correspond, in fact, to about the mean expansion velocity observed in ultraluminous infrared galaxies (Rupke, Veilleux, & Sanders 2002). Moreover, these velocities are comparable to or exceed the sound speed of $\sim 200 \text{ km s}^{-1}$ we derive for this hot gas. Therefore, the loops could be shocked swept-up ISM. If they are superbubbles blown by a violent localized starburst (e.g., at the nucleus of NGC 4039), as,

e.g., in the Tomisaka & Ikeuchi (1988) model, one would expect more of a bipolar outflow morphology. They could correspond to two separate events, with perhaps the receding sides of the outflows obscured by the main body of the emission from the merger. Another possibility that will need to be explored with hydrodynamical simulations, is that the loops are somehow connected with the merging process, as suggested in the case of Arp 220, where similar structures are observed with Chandra (McDowell et al. 2003). We note that a large-scale ring of hot gaseous emission is present in NGC 5128, a likely merger remnant (Karovska et al. 2002).

Given the long cooling times of both loops and halo in The Antennae, it seems possible that—if these features are bound by a dark massive halo—they may persist after the completion of the merger and the formation of the resulting elliptical galaxy. Interestingly, the total mass of hot gas in these extended features is $\sim 4 \times 10^8 M_{\odot}$. This mass is comparable with that reported from X-ray observations of relatively X-ray faint Elliptical and S0 galaxies (e.g., Roberts et al. 1991).

5. CONCLUSIONS

The above results demonstrate the power of sensitive, high-resolution X-ray observations. Thanks to a deep 411 ks observation of The Antennae, we now have a first picture of the varying chemical enrichment of the ISM, and we can see this hot medium expanding into the intergalactic space and possibly enriching the intergalactic medium with metals. Given the long cooling time of the extended halo, these observations may also show the formation of the hot halo of the elliptical galaxy that will be created by the merger. These data provide a new, welcome opportunity to witness the chemical evolution of galaxies in action, and offer a nearby glimpse of the distant evolving Universe.

We thank the CXC DS and SDS teams for their efforts in reducing the data and developing the software used for the reduction (SDP) and analysis (CIAO). We thank Martin Elvis and Larry David for useful discussions. This work was supported by NASA contract NAS 8-39073 (CXC) and NASA Grant G02-3135X. ARK gratefully acknowledges a Royal Society Wolfson Research Merit Award, and FS support from NSF grant AST-0205994.

REFERENCES

Baldi, A. et al. 2003, in preparation Barnes, J. E. 1988, ApJ, 331, 699 Breitschwerdt, D. 2003, RMxAC, 15, 311 Breitschwerdt, D. 2003, RMXAC, 15, 311
Fabbiano, G., Zezas, A., & Murray, S. 2001, ApJ, 554, 1035
Fabbiano, G., Zezas, A., King, A. R., Ponman, T. J., Rots, A., Raymond, J., & Schweizer, F. 2003a, ApJ, 584, L5
Fabbiano, G., King, A. R., Zezas, A., Ponman, T. J., Rots, A., Schweizer, F. 2003b, ApJ, 591, 843
Fabbiano, G., Krauss, M., Zezas, A., Rots, A., & Neff, S. 2003c, ApJ, Fabbiano, G. & Trinchieri, G. 1983, ApJ, 266, L5 Gilbert, A.M., 2002, PhD Thesis, University of California, Berkely Hibbard, J. E., van der Hulst, J. M., Barnes, J. E., & Rich, R. M. 2001, AJ, 122, 2969 Karovska, M., Fabbiano, G., Nicastro, F., Elvis, M., Kraft, R. P. & Murray, S. S. 2002, ApJ, 577, 114 Martin, C. L., Kobulnicky, H. A. & Heckman, T. M. 2002, ApJ, 574,

McDowell, J. C., et al. 2003, ApJ, 591, 154 Mihos, J. C., Bothun, G. D., & Richstone, D. O. 1993, ApJ, 418, 82 Navarro, J. F., Frenk, C. S., & White, S. D. 1995, MNRAS, 275, 56 Neff, S. G., & Ulvestad, J. S. 2000, AJ, 120, 670 Ponman, T. et al. 2003, in preparation Roberts M. S., Hogg, D. E., Bregman, J. N., Forman, W. R., Jones, C. 1991, ApJS, 75, 751

Rupke, D. S., Veilleux, S., & Sanders, D. B. 2002, ApJ, 570, 588 Smith, R. K., Brickhouse, N. S., Liedahl, D. A., Raymond, J. C. 2001, ApJ, 556, L91

Zooff, Aps., 536, Est. Tomisaka, K. & Ikeuchi, S. 1988, ApJ, 330, 695 Weisskopf, M., Tananbaum, H., Van Speybroeck, L. & O'Dell, S.

2000, Proc. SPIE 4012, p. 2 (astro-ph 0004127)
Whitmore, B. C., Zhang, Q., Leitherer, C., Fall, S. M., Schweizer, F., & Miller, B. W. 1999, AJ, 118, 1551 Wilson, C. D., Scoville, N., Madden, S. C., & Charmandaris, V. 2000,

ApJ, 542, 120 Zezas, A. & Fabbiano 2002, ApJ, 577, 726 4 Fabbiano et al.

Zezas, A., Fabbiano, G. Rots, A. H., & Murray, S., 2002a, ApJS, 142, 239
 Zezas, A., Fabbiano, G. Rots, A. H., & Murray, S., 2002b, ApJ, 577, 710

Zezas, A. et al. 2003, in preparation Zhang, Q., Fall, S. M., & Whitmore, B. C. 2001, ApJ, 561, 727

Table 1										
Best-fit (68% errors) an	D STELLAR PARAMETERS FOR THREE	REGIONS OF THE ANTENNAE ISM								

$Reg.^a$	χ^2/dof	$N_H (10^{21} \text{cm}^{-2})$	kT (keV)	$Z_{Ne} \ (Z_{Ne,\odot})$	$Z_{Mg} \ (Z_{Mg,\odot})$	$Z_{Si} \ (Z_{Si,\odot})$	$Z_{Fe} \ (Z_{Fe,\odot})$	$_{\rm (Myr)}^{\rm Age}$	Rel. SFR
$R1^b$	24.6/34	$0.18^{+0.73}_{-0.18}$	$0.18_{-0.05}^{+0.04} \\ 0.56_{-0.07}^{+0.05}$	$0.93^{+2.02}_{-0.67}$	$0.70^{+0.93}_{-0.54}$	< 0.25	$0.58^{+0.88}_{-0.27}$	4	0.4
R5	31.5/34	$0.08_{-0.08}^{+0.23} \\ 1.76_{-1.09}^{+0.70}$	0.30 ± 0.02	$7.88^{+1.43}_{-1.90}$	$16.91_{-4.25}^{+7.64} \\ 3.19_{-1.62}^{+4.97}$	$23.70^{+13.38}_{-10.73}$	$2.67_{-0.34}^{+1.06} \\ 0.78_{-0.41}^{+0.59}$	10.6	2.3
R7	83.2/73	$1.76^{+0.70}_{-1.09}$	$0.50^{+0.08}_{-0.10}$	$3.11_{-1.19}^{+4.15}$	$3.19^{+4.97}_{-1.62}$	$4.40^{+18.04}_{-2.41}$	$0.78^{+0.59}_{-0.41}$	4	1.0

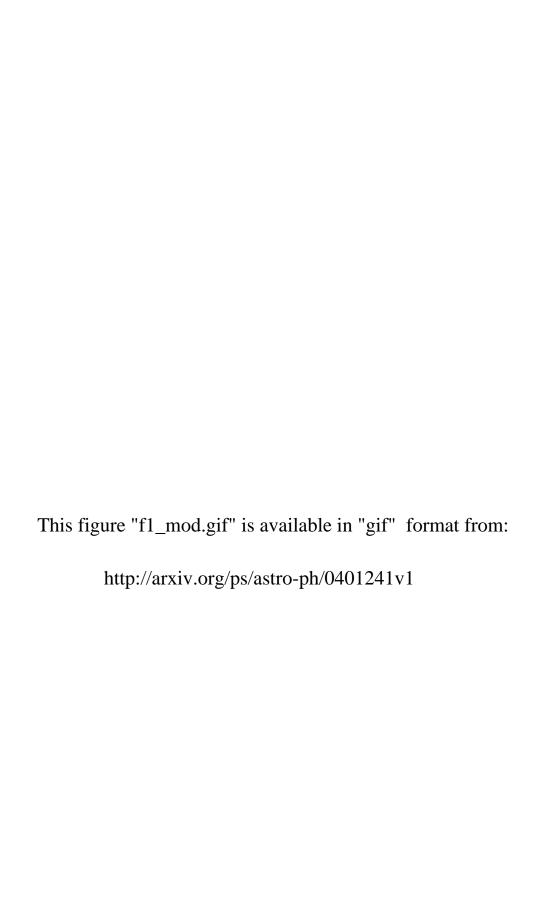
a) R1 and R7 are representative low and high abundance regions out of 21 regions studied in detail by Baldi et al. (2003). R5 is the region with the most extreme high abundances. These regions are identified by '1', '5' and '7' in fig. 3.
b) Two thermal components are required to fit the R1 data. While R1 consists of two areas, either one does not have enough counts for a meaningful fit. Both areas have similar X-ray colors, suggesting similar spectra.

Fig. 1.— Coadded astrometry-corrected 'raw' data (0.3-6 keV), together with a representative outline of the optical interacting disks (blue contours), and red contours derived from the Hubble WFPC-2 $H\alpha$ image (from Whitmore et al. 1999), that indicates the position of HII regions in the Antennae.

Fig. 2.— Exposure-corrected adaptively-smoothed true-color image, obtained from data in the 0.3-0.65 (red), 0.65-1.5 (green) and 1.5-6.0 keV (blue) energy bands. The data processing is similar to that followed in Fabbiano et al. (2003c) and is explained fully in Baldi et al. (2003, in preparation). The maximum significance has been set to 5σ , while the maximum smoothing scale corresponds to a minimum significance of 2.4 σ inside the optical body of the Antennae in the 'green' band. The same smoothing scales (1 - 128 pixels) were applied to the three bands. The color scale has been stretched to allow the display of both the large-scale diffuse emission and the luminous, more resolved features.

Fig. 3.— Metallicity map of the hot ISM of The Antennae, where red, green, and blue indicate emission by Fe, Si, and Mg respectively. Continuum was subtracted by estimating the contribution of the overall best-fit two-component thermal bremsstrahlung model in the two bands at 1.4-1.65 keV and 2.05-3.50 keV, where no strong lines are observed. Point-like sources were excluded, following Fabbiano et al. (2003c). The Fe-L band image was adaptively smoothed to a significance between 3σ and 5σ , and the same scales were applied to the other line images.

Fig. 4.— ACIS spectrum of region R5, together with best-fit model and fit residuals. Gain corrections were applied using software provided by the CXC Calibration Group.



This figure "f2.gif" is available in "gif" format from:

This figure "f3.gif" is available in "gif" format from:

This figure "f4_mod.gif" is available in "gif" format from:

This figure "f5.gif" is available in "gif" format from: